# A mechanical characterization of unfired dry earth: ultimate strength, damage and fracture parameters

Stefano Lenci[1], Quintilio Piattoni[1], Francesco Clementi[1], Tomasz Sadowski[2]

[1]*Department of Architecture, Building and Structures Polytechinic University of Marche, Ancona, Italy*

*E-mail*: *lenci @univpm.it, francesco.clementi@univpm.it*

[2]*Department of Solid Mechanics, Lublin University of Technology, Lublin, Poland*
*E-mail*: *t.sadowski@pollub.pl*

*Keywords:* Earth blocks, Compressive strength, 3-points bending, Damage, Fracture characteristics.

SUMMARY. In this paper, compression and three-points bending tests were conducted for a particular composition of unfired dry earth. The results obtained from mechanical tests are presented in the form of stress-strain diagrams. The tests are performed by displacement control, so that the softening behavior can be detected. The most important purpose of this study consists of the analysis of the non-standard properties like damage and fracture characteristics. These are determined for different geometries and aspect-ratios, and partially with the help of Finite Element Method analyses which are required to extract the relevant parameters from the experimental data. Finally, the results show that the considered material may support large deformations after reaching the maximum load.

## 1 INTRODUCTION

For many centuries hand moulded earth blocks have been used for load-bearing masonry structures, including constructions which are outstanding from a structural point of view, such as the well-known 10-storey buildings in Yemen [1]. In the imperial age of Rome these structures were done yet. Such earth blocks were readily produced by manual compaction and theirs content can vary, depending on the building site.

After the Roman era and in the middle age, the construction of house with earth became marginal in western countries, because it required an able labour to create adequate blocks, because it became non competitive with respect to other construction materials (masonry of fired clay bricks first, and then steel and concrete), both in terms of costs and mechanical properties, and because of the impossibility to standardise the composition of material due to the local variations.

Over the past seventy years the use of earth block experiences a sort of revival, and they have been re-developed or "re-discovered," and increasingly used. On the contrary, compressed hearth blocks were continuously used in developing countries, because earth is cheap, environmentally friend and abundant. Today the world heritage is very rich in all countries of earth constructions, and it is estimated that approximately 30% of the world population still lives in earthen structures [2]. In fact, the use of local materials, in general, and of earth block, in particular, in building of houses is one of the ways to support durable development of the entire planet, because this meets

the needs of the present without compromising the ability of future generations to meet their own needs [3, 4].

This trend call for a determination of the mechanical properties on earth blocks, which is the starting point for a modern use of this old material, according to the current standard safety requirements. Quality control of the compressed earth blocks is also an important issue, and today testing procedures are available and easily performed in a civil engineering laboratories [5, 6].

Great attention has been paid to the experimental determination of the compressive strength, as it represents the most important parameter to evaluated the load-bearing properties [7-10]. A simple model to compute the compressive strength by means of a three point bending test has been proposed in [5], and the results have been compared with experimental data. Results from compression tests at different ages was reported in [11] (24h, 7 and 28 days after construction) and [12] (7, 14, 21 and 28 days after construction). The matter of how properly perform a compression test has been deeply analyzed and reviewed in [6], where the influence of the block geometry, of the test procedure (including those proposed by international standards) and of the basic material properties (dry density, cement and moisture contents) have been discussed.

The effect of reinforcing fibers, both natural (straw) and artificial (plastic and polystyrene) inserted in the earth block as a fabric layers are investigated in [13] and [14], while Yetgin *et al.* [15] have shown that the addition of straw fibers decrease the compressive strength, a result which is confirmed by [16]. In [15] also tensile tests were performed. Some indications on the compressive strength of rammed earth and adobe are reported in the appendix of [17], together with some suggestions on the safety factors to be used. It is also shown how the compressive strength increase by the use of added cement and/or lime. The effect of stabilization with added cement was also considered in [18].

Although to a minor extent, also bending test have been performed, and the flexural ultimate stress has been determinated [5, 12, 16, 18], with results showing that it varies from 1/5 to 1/20 of the compressive strength [17], and that it is much more influenced by various parameters such has percentage of straws.

On the contrary, up to the authors' knowledge, less or no attention has been paid to other important properties, such as damage [19] or fracture properties, which constitute one of the objectives of this paper. Our interest lies in understanding the properties of rammed earth, with the subsequent aim of improving its strength and durability when used for load-bearing walls, and we report on results obtained from an experimental campaign performed at the "Laboratorio Prove Strutture e Materiali" of the Polytechnic University of Marche at Ancona, Italy.

The damage properties are discussed with reference to two different specimens, compressed cubes and prisms, in order to investigate the effect of the aspect ratio (Sect. 3). Then, the fracture properties have been discussed with a three point bending test (Sect. 4). In order to achieve information also on the flexural strength of the material, we have considered a virgin specimen, i.e., without an initial crack or notch. Then, to further assess the fracture characteristics of the material, we have also considered a specimen with an initial crack. The results of the experimental tests have been paralleled by numerical simulations performed with finite element method to single out the desired fracture parameters.

## 2 MATERIALS AND PREPARATION

The material used to realized the compressed earth block is made of three different constituents, having the following proportions: 1 volume of "earth," 1/2 volume of "sandstone" and 1/2 volume of fibres straw.

The geotechnical characteristics of the "earth" are reported in Fig. 1a (particle size distribution) and in Tab. 1 (physical properties). According to the ASTM D2487 it can be classified as "lean clay with sand (CL)." The geotechnical characteristics of the "sandstone" are reported in Fig. 1b (particle size distribution) and in Tab. 1 (physical properties). According to the ASTM D2487 it can be classified as "well graded sand (SW)." The fibres straw has a length which varies from 2 to 8 cm, with an average valued of 5 cm.

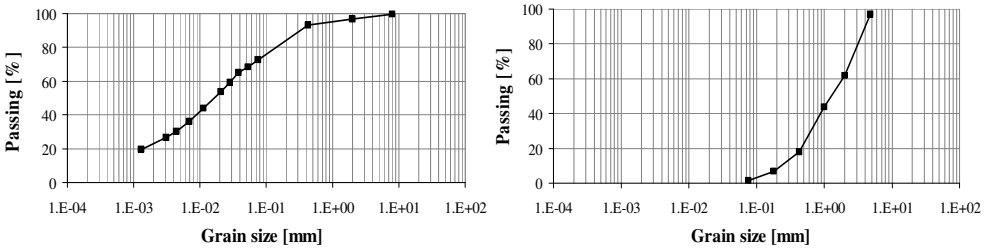


(a) (b)

Figure 1. Grading curve for (a) the "earth" and (b) the "sandstone."

| | "earth" | "sandstone" |
|---|---|---|
| Clay (%) | 22.4 | 0.5 |
| Silt (%) | 49.9 | 1 |
| Fine sand (%) | 24.5 | 61.8 |
| Coarse sand (%) | 3.2 | 36.7 |
| Liquid limit (%) | 26.4 | |
| Plastic limit (%) | 18.4 | |
| Plastic index (%) | 8 | |

Table 1. Physical properties.

Material preparation and mixing was carried out manually. 1/3 (on average) volume of water was added to guarantee normal consistency and manual operations. The mixture was manually pressed into formworks of wood of the dimensions of 32×46×13 cm. After removing the boxes, the blocks were cured under stationary thermo-hygrometric conditions (temperature 23-26 °C; relative humidity 45-55%). After about five months, the blocks were cut by saw to obtain the desired specimens. At the end of the tests, it was verified that the moisture contents was less than 3-4%, so we have actually tested a dry material.

## 3 COMPRESSION TESTS

As the compressive strength depends on the dimension of the specimen, and because this matter is still under investigation and it is not definitely established the influence of the aspect ratio [6], we decide to perform compression tests on cubic (Fig. 2a) and prismatic (Fig. 2b) specimens.

The procedure adopted is that of national standards and codes of practice for fired clay and concrete blocks. Specimens are capped and tested directly between steel plates. Blocks surface are always sufficiently flat and parallel that only thin layer of sand capping is necessary. In order to detect the softening branch, we have applied a controlled displacement and measured the force, i.e.

a soft device was used. For each specimen dimension, we have performed two tests. The first one is monotonic and is aimed at capturing the general overall behaviour, including the determination of the Young modulus $E$, of the maximum stress $\sigma_{max}$ and of the ultimate strain $\varepsilon_u$. The second one is cyclic, and from this case we detected the damage behaviour of the material.

(a) (b)

Figure 2. The specimens for the compression tests: a) cubic 50×50×50 cm, b) prismatic 45×58×112 cm.

3.1 *Cubic samples*

The result of the monotonic compression tests are reported in Fig. 3.a. The maximum stress $\sigma_{max}$=1.57 MPa and the Young modulus $E$=148.08 MPa are in agreement with the results of other studies (see, e.g., [15]). Also the values of the strain in correspondence of $\sigma_{max}$ is comparable with that obtained by other authors (see, e.g., [15]). What was not reported in other papers is the long softening branch, which highlight the very large deformation sustained before collapse, which is of course a consequence of the presence of the fibres of straw. Note that the ultimate strain $\varepsilon_u$=20.8 % is comparable to that of steel. This sort of "ductility" is very important in terms of new trends for computing the seismic resistance of buildings.

The cyclic test permits evaluating the damage of the material. The relation between the stress and the strain (Fig. 3.b) shows that the compressive strength, the overall shape of the curve and the initial Young modulus are comparable, but the final strain is approximately halved respect to that of the monotonic test. Thus, the damage has not only an influence on the developing elastic modulus, but also on the "ductility."

After the first step the compression causes a compacting of the sample, so that initially the elastic modulus increases considerably. It becomes 4 time larger at the end of the linear elastic range, where we have performed the first unload-reload cycle. In subsequent cycles the damage of the specimen entails the reduction of the Young's modulus, which is evident in Fig. 3.b.

The damage behaviour of the material is detected by the scalar damage parameter [20]

$$d = 1 - (E_a/E_i), \tag{1}$$

where $E_a$ is the elastic modulus of the current step of load and $E_i$ is the initial elastic modulus, where we have disregarded the $E$ of the virgin state and have considered the "initial" value of $E$ that after the compacting.

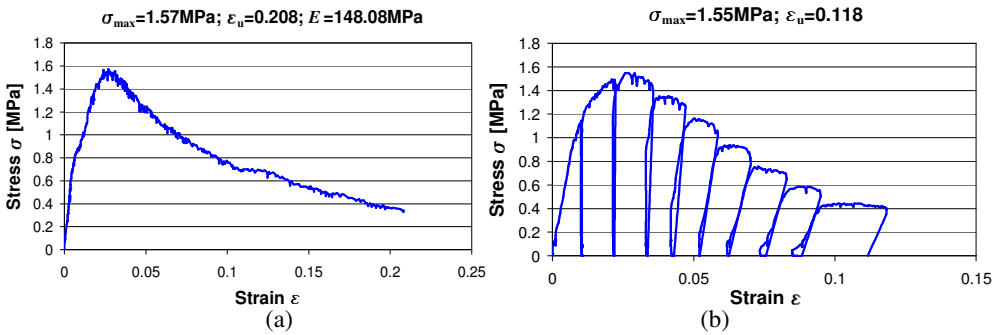


(a) (b)

Figure 3. a) Stress-strain relation for the monotonic compression test on cubic specimen, b) Stress-strain relation for the cyclic compression test on cubic specimen.

The damage coefficient as a function of the residual stress at the end of the unload process is reported in Fig. 4, together with the interpolating curve

$$d = 0.0007\varepsilon_4 - 0.0161\varepsilon_3 + 0.1104\varepsilon_2 - 0.0891\varepsilon, \quad (2)$$

which gives $R^2 = 0.9898$ and therefore it is very accurate. From Fig. 4 it is seen that the damage increases rapidly in the softening path of the stress-strain curve (compare Figs. 3b and 4), and that it quickly tends to the completely damage state ($d = 1$). For example, for $\varepsilon = 0.05$, i.e. when the stress in still about 80% of the maximum stress (Fig. 3.b), that damage is about 0.8 (Fig. 4), i.e. the material is almost completely damaged while still having a good stress resistance.

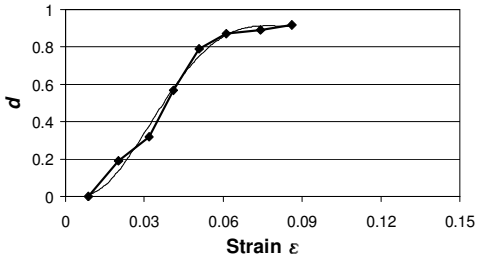


Figure 4. The scalar damage parameter as a function of the strain ε (thick line), and the interpolating curve (thin line) for the cubic specimen.

3.2 *Prismatic samples*

The experimental stress-strain relation for the monotonic test on the prismatic sample is reported in Fig. 5.a, where the corresponding curve of the cubic sample (Fig. 2.a) is also reported for comparison. We see that with the prismatic sample we have a slightly higher maximum stress, and the same Young modulus. The main differences, both qualitative and quantitative, are in the softening branch, that of prismatic sample being much more (approximately one half) shorter. Thus, the "ductility" is lost by the prismatic sample. This can be explained by the different rupture mechanism observed in the two cases. In fact, for the cubic specimen we have a spread cracking at breaking, so that a lot of energy is spent to break the material, while for the prismatic specimen we

have seen only one diagonal crack, i.e. a localized rupture requiring less energy and thus developing in a easier way, i.e., for lower values of the strain. This is a noteworthy "size effect" observed in our tests.

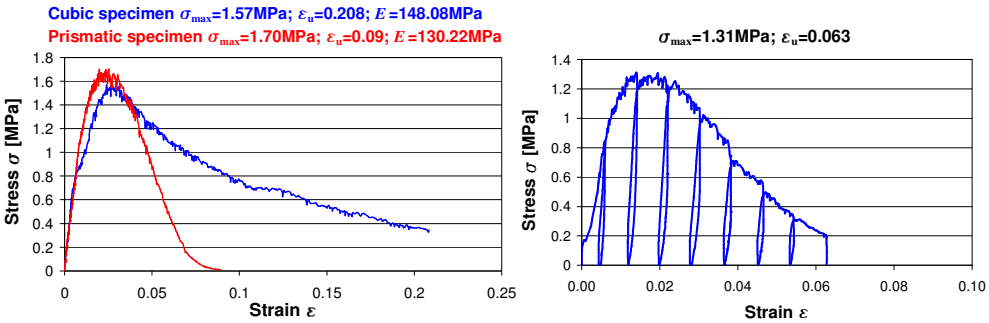


(a) (b)

Figure 5. a) Stress-strain relation for the monotonic compression test on prismatic and cubic specimens, b). Stress-strain relation for the cyclic compression test on prismatic specimen.

The result of the cyclic compression test is reported in Fig. 5.b. We have that the maximum stress has been reduced with respect to the monotonic test ($\sigma_{max}$=1.31 MPa vs $\sigma_{max}$=1.70 MPa), while the initial Young modulus is almost unchanged ($E$=129.32 MPa vs $E$=130.22 MPa). As in the case of cubic specimen, there is a initial compacting phase, where the elastic modulus strongly increases before undergoing damage. Contrarily to the cubic specimen, however, the overall softening branch has not been strongly modified in the cyclic test.

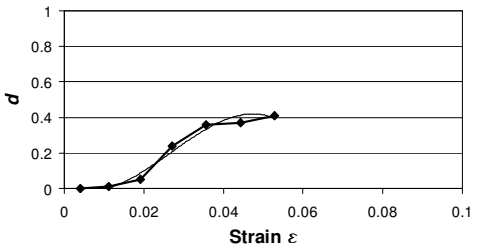


Figure 6. The scalar damage parameter as a function of the strain ε (thick line), and the interpolating curve (thin line) for the prismatic specimen.

The damage parameter are reported and in Fig. 6. The interpolating curve is

$$d = 0.0012\varepsilon_4 - 0.0231\varepsilon_3 + 0.1254\varepsilon_2 - 0.1132\varepsilon \quad (3)$$

with $R^2$ = 0.9733. When compared with Fig. 4, the Fig. 6 shows that for the prismatic test the development of damage is minor, and it tends to the final value of $d$ = 0.4, which means that at the rupture the damage is less than one-half. Thus, the lost of "ductility" is balanced by the increment of the undamaged features at breaking.

## 4 THREE-POINTS BENDING TESTS

These tests have been performed on specimens obtained from the same block used to make the specimens for the compression tests. So in addition to the same composition, they have the same content of water after five months of the drying process. The equipment is the same, and we have used also two transducers of horizontal displacement. The specimens of dimensions $L'$ = 355 mm (length), $B$ = 85 mm (width) and $W$ = 112 mm (height) are put on two steel rollers that are free to roll. The distance between the lower rollers is $L$ = 255 mm.

The monotonic test has been done by applying the vertical displacement $\delta^V$ in the middle of the upper side of the sample, and by recording the value of the vertical force $F$ by a load cell. The experimental $F$- $\delta^V$ curve is plotted in Fig. 7.a.

Figure 7.a shows that the initial elastic range, which can be approximated quite well by a linear path, ends at $F = F^V_{max}$= 2274 N and $\delta^V$= 1.239 mm. As the beam theory does not apply because the specimen is not slender enough, we have used the Finite Element Method (FEM) to correlate these data. In the FEM computations care is used in proper modelling of the roller pressure, as the problem is sensitive to the stress localization around the rollers.

From the FEM analysis we obtain $E$ = 145 MPa and $\sigma_{max}$ = 0.75 MPa (the Poisson coefficient used in the FEM is $\nu$=0.3). Note that with the beam theory we would get $E = FL^3/(4\delta^V BW^3)$ = 63.7 MPa and $\sigma_{max} = 3FL/(2BW^2)$ = 0.82 MPa, the former being clearly not adequate. While $E$ = 145 MPa is in very good agreement with the Young modulus computed by the compressions tests, $\sigma_{max}$ = 0.75 MPa provides an estimate of the tensile (flexural) strength of the material, which is in good agreement with the value $\sigma_{trac}$ = 0.5÷0.8 MPa obtained in [15] by a direct traction test.

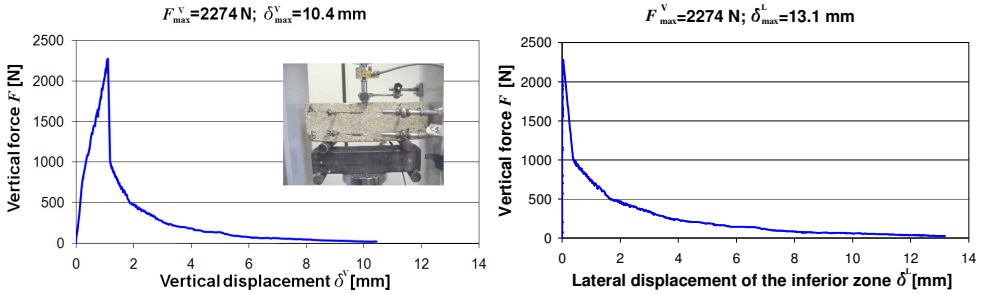


(a) (b)

Figure 7. The measured vertical force $F$ versus: a) the applied vertical displacement $\delta^V$ for the monotonic 3-points, b) the measured horizontal displacement of the lower part of the sample.

After the initial elastic range, an almost vertical crack appeared in the middle of the lower side, for the vertical displacement $\delta^V$ = 1.315 mm. It then suddenly propagates toward the upper side. During the crack propagation a relatively long softening branch is observed (Fig. 7.a), with a final vertical displacement equal to $\delta^V_{max}$= 10.4 mm. The Crack Mouth Opening Displacement (CMOD) measured at the end of the test is approximately equal to 17 mm.

The softening branch and the large final CMOD is also highlighted by the curve of Fig. 7.b, which reports the measured horizontal displacement in the lower part. The maximum lateral displacement $\delta^L$ is 13.1 mm, which is lower than 17 mm because the displacement is measured at about 1/5 of the height and not at the bottom.

The results of the cyclic bending test are reported in Fig. 8. The initial elastic range is the same as in the monotonic test, as well as the overall shape of the softening branch, which however in

this case has been stopped for a smaller value of the vertical displacement. There is a decrease in the slope of the unloading-reloading paths, which however leaves some permanent deformations. Thus, this damage is not only due to the main propagating crack, which of course reduces the stiffness of the specimen, but also to an "intrinsic" and spread damage of the material.

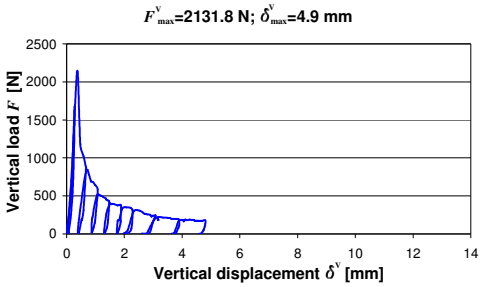


Figure 8. The measured vertical force F versus the vertical displacement $\delta^V$ for the cyclic three points bending test.

*4.1. Fracture characteristics and parameters*

In this section we apply the fracture mechanics concepts [21] to describe the experimental results and to determine the fracture characteristic of the material. It is supposed that the material is brittle enough so that the Linear Elastic Fracture Mechanics [21] can be applied with sufficient accuracy. In the 3-points bending test we are dealing with the mode I, so that the most important parameter is the stress intensity factor $K_I$, which for the specimen of Fig. 7.a is given by [21]

$$K_I = \frac{FL}{BW^{3/2}}\left[2.9\left(\frac{a}{W}\right)^{1/2} - 4.6\left(\frac{a}{W}\right)^{3/2} + 21.8\left(\frac{a}{W}\right)^{5/2} - 37.6\left(\frac{a}{W}\right)^{7/2} + 38.7\left(\frac{a}{W}\right)^{9/2}\right], \quad (4)$$

where $a$ is the crack length measured from the bottom.

Since LEFM is assumed to apply, the crack propagation occurs under the condition $K_I = K_{Icr}$. To fulfil exactly the experimental data, we assume that $K_{Icr}$ is a function of the crack length $a$, $K_{Icr} = K_{Icr}(a)$, and determine this function, called $R$-curve [21, 22], with the following procedure.

The elastic constants are equal to: $E$ = 145 MPa and $\nu$=0.3. For each imposed value of $\delta^V$ of the softening branch of Fig. 7.a, we enter the FEM with an arbitrary $a$ and the applied vertical displacement $\delta^V$. Then, we vary $a$ until the force obtained by the FEM becomes equal to the force experimentally measured (Fig. 7.a). Then we get correlation $a = a(\delta^V)$, which provides an estimation of the crack length as a function of the applied vertical displacement. With this function and the experimental curve $F = F(\delta^V)$ one can compute $F = F(a)$ by eliminating the vertical displacement $\delta^V$. Introducing the function $F$(a) into equation (4) we get finally the desired $K_{Icr}(a)$. The curve $a(\delta^V)$ is reported in Fig. 9a, while the $R$-curve $K_{Icr}(a)$ is given in Fig. 9b.

From Fig. 9a we can see that the crack starts at $\delta^V$ = 1.315 mm, where it suddenly reaches the length $a/W$ = 0.47, i.e., almost the half of the height, so that the specimen is rapidly damaged. Then it continues to increase, and at $\delta^V$ = 3 mm it reaches the values $a/W \cong 0.80$ with a FEM computed CMOD = 4.62 mm. After this point the crack continues to growth with a decreasing slope up to the final value which is estimated to be about $a/W$ = 0.90. Due the large extension of the crack both the experiments and the FEM simulations becomes unreliable in this final range,

mainly because of the interactions between the stress concentration at the crack tip and the stress concentration just below the upper roller. This fact is confirmed by Fig. 9b, where we observe a non-monotonic behaviour of the *R*-curve for $a/W>0.75$. At this point the material toughness reaches its maximum, and further deformation lead to the $K_{Icr}$ decrease. It is necessary to point out the fact that the real crack is not rectilinear, so that the simulations based on rectilinear crack would be in any case approximate particularly at the final stage of deformation process.

It is worth to remark that the previous one is an *unstable* crack propagation, which is seen only because we applied displacements and measure the forces.

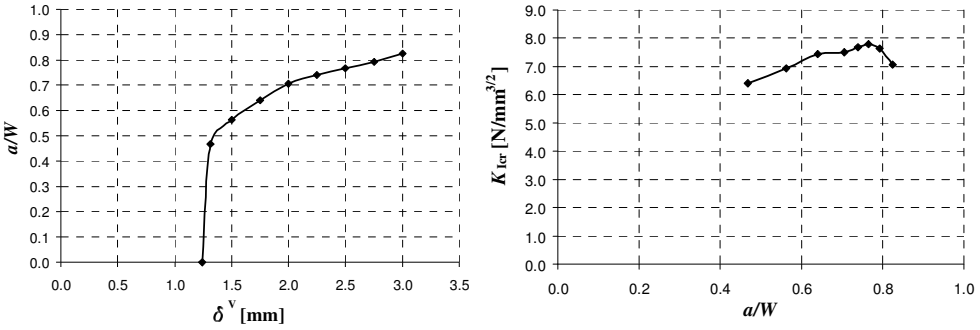


(a) (b)

Figure 9. The FEM estimated: a) $a(\delta^V)$ curve, b) $K_{Icr}(a)$.

From the Fig. 9b we see that the critical stress intensity factor is a varying function of the crack length, monotonic in the most reliable part of the diagram. However, in the range $0.47 < a/W < 0.85$ it can be roughly approximated by the average value $K_{Icr} = 7.2$ N/mm$^{3/2}$, which provides an estimate of the crack resistance of the considered earth material.

*4.2. The specimen with an initial crack*

To further assess the fracture characteristics of the material, we have performed another three points bending test on a specimen with an initial crack (Fig. 10). Here we have considered a slightly different material composition (1 volume of "earth," 1/2 volume of "sandstone" and 3/4 volume of fibres straw) and a slightly different geometrical dimensions ($L' = 360$ mm, $L = 320$ mm, $B = 84$ mm and $W = 113$ mm).

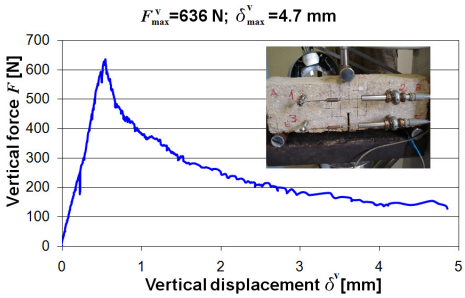


Figure 10. The measured vertical force versus the applied vertical displacement $\delta^V$ in the monotonic three points bending test for the specimen with initial crack.

The initial crack length is $a_0$ = 44 mm, i.e., $a_0/W$=0.4. The experimental data for the monotonic test are presented in Fig. 10. From this figure we can see that there is no longer the sudden jump as in Fig. 7.a, and the propagation is continuous and starts at $F = F^{V}_{max}$= 636 N and $\delta^{V}$ = 0.544 mm. Furthermore, the initial crack now induces an almost rectilinear propagation of the crack.

The analysis of this case is analogous to that of the previous subsection. From the initial straight path we get $E$ = 245 MPa (and we still assume $\nu$=0.3 in the FEM simulations), while elaborating the descend path we obtain the $a(\delta^{V})$ and the $R$-curve $K_{Icr}(a)$ which are reported in Fig. 11.a and 11.b, respectively.

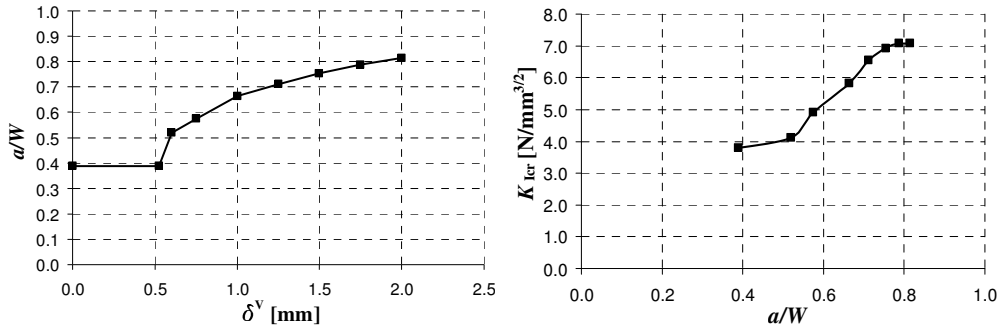


(a) (b)

Figure 11. The FEM estimated: a) $a(\delta^{V})$ curve, b) $K_{Icr}(a)$ for the specimen with an initial crack.

The classical square root shape [21] of the $a(\delta^{V})$ curve for $a(\delta^{V})\rightarrow a_0$ is clearly visible in Fig. 11.a, according to the fact that there is no an initial sudden jump in this case.

In the initial part of the Fig. 11.b there an almost constant behaviour of the $R$-curve, which is related to the initial, smooth propagation of the crack. Successively, when the crack propagation becomes steady, the $R$-curve approaches an almost constant slope.

In this case the average value of the critical stress intensity factor is $K_{Icr}$ = 5.8 N/mm$^{3/2}$, which is slightly lesser than that of the previous case. However, the differences are modest and can be justified by statistical considerations.

## 5 CONCLUSIONS

The basic mechanical characteristics of the unfired dry earth have been investigated by different experimental tests. Namely the compression of cubic and prismatic samples, and three-points bending tests were performed. The aim of this paper was the investigation of the elastic parameters and strength proprieties, their dependence on the aspect ratio, and others (non usual) materials characteristics like damage and fracture resistances. The compression tests have shown that the increment of the aspect ratio make the specimen less “ductile.”

Both monotonous and cyclic applied displacements were considered. The former cases were used to determine the “classical” parameters such as Young’s modulus and compressive strength, which are seen to be comparable to those reported in the literature. The latter case is used to determine the scalar damage parameter $d$ of the samples, in particular of cubic and prismatic specimens, which have been shown to have the same qualitative behaviour but a quite different quantitative behaviour.

We have highlighted the long softening branches experienced by all the specimens, which shows the very large deformation sustained before collapse. These properties, which are not

reported in the literature, are a consequence of the fibres of straw presence inside the material and they are very important for building design.

Finally, we have investigated the fracture behaviour. This was done by considering the material brittle enough so that the LEFM can be applied with sufficient accuracy. We have analysed two different three-points bending tests, one without and one with the initial crack. In both case we have determined the *R*-curve of the material, i.e., it resistance to crack propagation, and have proposed some average values to be used in first approximation analysis.

In conclusion, we have deduced the generic mechanical properties of rammed earth, some already present in literature and others news, which are needed for understanding the behaviour of some bigger structural elements constructed with this kind of material.

## 6 ACKNOWLEDGEMENT

The authors wish to gratefully acknowledge the valuable assistance of the Laboratory technicians Franco Rinaldi, Umberto Taddei and Andrea Conti. The help of the Geotechnical Laboratory of the Polytechnic University of Marche is also acknowledge.
The authors wish to express their gratitude to: 1) 6 Framework Programme of the European Union for the support within the project MTKD-CT-2004-014058 (Marie Curie – Transfer of Knowledge) and 2) Polish Ministry of Science and Higher Education for the support within the grant No No 65/6.PR UE/2005-2008/7.

*References*

[1] Houben H, Guillaud H. Earth construction: a comprehensive guide. London: IT Publications (1994).

[2] Cofirman R, Agnew N, Auiston G, Doehne E. Adobe mineralogy: characterisation of adobes from around the world. In: 6th international conference on the conservation of earthen architecture, Las Cruces, NM; 14-19 October (1990).

[3] The World Commission on Environment and Development (The Brundtland Commission). In: Press OU, editor. Our common future. O. U. Press (1987).

[4] Morel J-C, Mesbah A, Oggero M, Walker P. Building houses with local materials: means to drastically reduce the environmental impact of construction. Building Environment; 36(10): 1119-26 (2001).

[5] Morel JC, Pkla A. A model to measure compressive strength of compressed earth blocks with the '3 points bending test', Construction and Building Materials; 16: 303-10 (2002).

[6] Morel JC, Pkla A, Walker P. Compressive strength testing of compressed earth blocks, Construction and Building Materials; 21: 303-9 (2007).

[7] Walker P. Strenght and durability testing of earth blocks. In: Proc. of the 6th international seminar on structural masonry for developing countries: 111-18 (2000).

[8] Walker P. Characteristics of pressed earth blocks in compression. In: Proc. of the 11th international brick/block masonry conference, Shangai, China, 14-16 october; 1997: 1-10.

[9] Hakimi A, Yamani A, Ouissi H. Rapport: resultats d'essais de resistance mecaniques sur echantilons de terre comprimee. Mater Constr; 29: 600-8 (1996).

[10] Heathcote K. Compressive strength of cement stabilized pressed earth blocks. Build Res Inf; 19: 1001-5 (1991).

[11] Lilley DM, Robinson J. Ultimate strength of rammed earth walls with openings, Proc. Instn Civ. Engrs & Bldgs; 110: 278-87 (1995).

[12] Medjo Eko R, Mpele M, Dtawagap Doumtsop M, Seba Minsili L, Wouatong AS. Some hydraulic, mechanical, and physical characteristics of three types of compressed earth

blocks. Agricultural Engineering International: the CIGR Ejournal; VIII: Manuscript BC 06 007 (2006).
[13] Binici H, Aksogan O, Shah T. Investigation of fibre reinforced mud brick as a building material. Construction and Building Materials; 19: 313-8 (2005).
[14] Binici H, Aksogan O, Nuri Bodur M, Akca E, Kapur S. Thermal isolation and mechanical properties of fibre reinforced mud bricks as wall materials. Construction and Building Materials; 21: 901-6 (2007).
[15] Yetgin S, Cavdar O, Cavdar A. The effects of the fiber contents on the mechanic properties of the adobes. Construction and Building Materials; 22: 222-7 (2008).
[16] Bouhicha M, Aouissi F, Kenai S. Performance of composite soil reinforced with barley straw. Cement and Concrete Composites; 27: 617-21 (2005).
[17] Delgado MCJ, Guerrero IC. Earth building in Spain. Construction and Building Materials; 20: 679-690 (2006).
[18] Mattone R. Unfired earth, traditions and innovations. L'industria dei Laterizi; 71: 313-20 (2001).
[19] Hakimi A, Fassi-Fehri O, Bouabid H, Charif D'ouazzane S, El Kortbi M. Comportament mecanique non lineaire du bloc de terre comprimee par couplage elasticite endommagement. Mater. Constr; 32: 539-45 (1999).
[20] Lemaitre J. A course on Damage Mechanics. Berlin: Springer (1996).
[21] Broek D. Elementary fracture mechanics. Sijthoff & Noordhoff (1978).
[22] Felten F, Schneider GA, Sadowski T. Estimation of *R*-curve in WC/Co cermet by CT test. Int. J. Refractary Metals & Hard Materials; 26: 55-60 (2008).